ISSN: 3144-1890

Wissen PUBLICATION GROUP

Journal of
Advanced Physics and Interdisciplinary Science

Review Article

Volume: 1 | Issue: 1 | November 2026 | Pages 01–17

Building a New Chemical Framework for a High T_C Superconductor Using Promising Elements

Clifford M Krowne, Emeritus

[1]Materials Physics & Chemistry Section, Materials and Sensors Branch, Material Science & Technology Division, and Microwave Circuits & Electromagnetic Theory Sections, Microwave Technology & Electromagnetics Branches, Electronics Science & Technology Division, Naval Research Laboratory, Washington, DC 20375, United States of America

[2]Chief Research Scientific Officer, Ashlawn Energy, LLC, 710 Resende Road, Bldg. 199, Webster, New York 14580, United States of America

***Corresponding Author:** Clifford M. Krowne, Materials Physics & Chemistry Section, Materials and Sensors Branch, Material Science & Technology Division, and Microwave Circuits & Electromagnetic Theory Sections, Microwave Technology & Electromagnetics Branches, Electronics Science & Technology Division, Naval Research Laboratory, Washington, DC 20375, United States of America.

Submitted: 30 October 2026 **Accepted:** 09 November 2026 **Published:** 20 November 2026

Citation: Krowne, C.M. (2026). Building a New Chemical Framework for a High T_C Superconductor Using Promising Elements. Journal of Advanced Physics and Interdisciplinary Science, 1(1), 01-17. DOI: https://doi.org/10.67927/JAdvPhysInterdiscipSci/2026(1)111.

Abstract

New uses and arrangements of the elements for making crystallographic unit cells which may superconduct, are proposed based upon the underlying physics, the solid state physical chemistry, and crystallographic growth methods. It is hoped that the ideas presented here will inspire a quest to reach considerably higher superconducting critical temperatures T_C than previously obtained at standard temperature and pressure conditions. To be economically viable and adapted by the energy community, realistically high T_C's must be found, and amenable to crystallographic growth using either old or new methods of preparation. Furthermore, the prepared SCs must allow ready fabrication into useful carriers of electrical power in such venues as power grid cables.

Keywords: Crystallographic Unit Cells, Superconductor, Electrical Power.

Introduction

The highest critical temperature superconductors with any possibility of operating at standard conditions with room temperatures and pressures (STP), requires overcoming a major hurdle. This hurdle is the presently highest T_C materials working at a nominal value of 135 K. This is about 165 K below room temperature, taken as nominally 300 K. This is completely an unacceptable situation. In order to move the entire field of superconductivity in the high temperature realm to realistically useful T_C values, herein are proposed a few new crystal structure possibilities, employing a new suit of elements to construct the unit cells of the crystal structures for the superconducting materials. The next sections of the paper are arranged as follows: II.: Informed by Examination of Carrier Transport Semiconductor Bandtsructures; III. Possible Elements for SC: Informed by High Power Electronics and Examination of Their Semiconductor Band structures; IV. Atomic Substitution of Oxygen with Either N or C Atoms; V. Substitutional Replacement of the Charge Sharing Atoms Interacting with the Conducting Tracks; VI. Substitutional Replacement of the Conducting Track Atoms; VII. Examination of the Critical Temperature from the Cooper Instability Equation; VIII. Conclusions.

Possible Elements for SC: Informed by Examination of Carrier Transport Semiconductor Band Structures

One wonders which elements might assist in raising the critical temperature for superconductors. An insight comes from a completely different area of high-power electronics. Previously, in semiconductor technology used for processing semiconductor devices like diodes and transistors, silicon and germanium have been employed, with silicon by far the most utilized semiconductor material. Associated with the fabrication of transistor monolithic integrated circuits, is the use of silicon dioxide as an insulating material. Furthermore, in the preparation of high frequency, high power transistors, including the fabrication of high electron mobility transistors (HEMTs), these radio frequency (RF) devices have moved from compound binary semiconductors such as GaAs to GaN and SiC.

Bandgap of GaAs is E_g =1.42 eV, and the bandgap is direct, in that the energy movement from valance band to conduction band states, requires no change in the momentum state of the transferring electron (Figure. 1) [1,2]. Besides use in transistor technology, GaAs is used in making solar cells. GaAs is a highly utilized material, but there was a movement to obtain

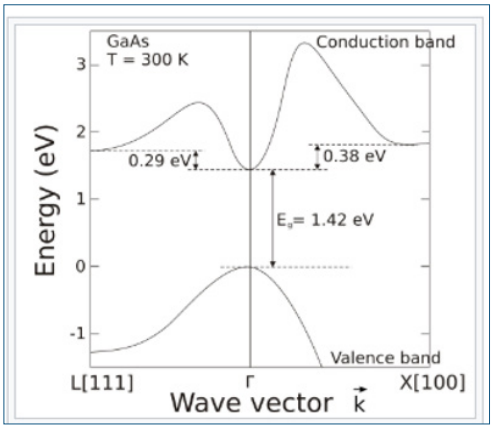

Figure 1: GaAs band structure showing energy vs wavevector in k-space. Seen are its variation in two of the major orthogonal crystallographic directions, the [111] and [100] directions. (a) from I. Vurgaftman, J. R. Meyer L. R. Ram-Mohan, "Band parameters for III-V compound semiconductors and their alloys," J. Appl. Phys. 89 (11),1 June 2001 [2].

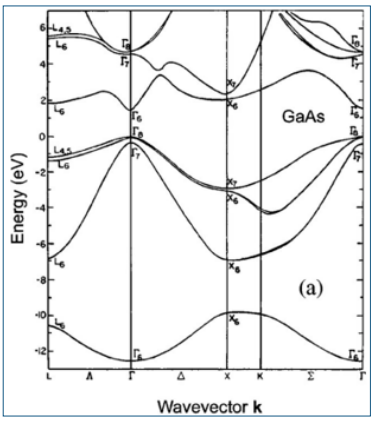

Figure 1: (b) From S. M. Sze, Physics of Semiconductor Devices, Wiley 1969 [1,2]. (c) from [3].

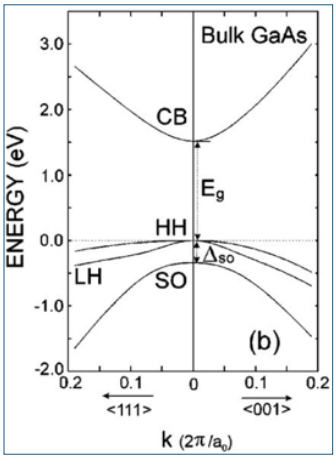

Figure 1: (c) From I. Vurgaftman, J. R. Meyer L. R. Ram-Mohan, "Band Parameters for III-V Compound Semiconductors and their Alloys," J. Appl. Phys. 89 (11),1 June 2001 [1].

One may wonder how the bandgap of GaAs compares to silicon. The bandgap of silicon is E_g =1.12 eV, [2,3]. Its band structure diagram is shown in Figure. 2. It is an indirect bandgap semiconductor, with the Fermi level set to $E_F = 0$ in the diagrams. The Fermi level is

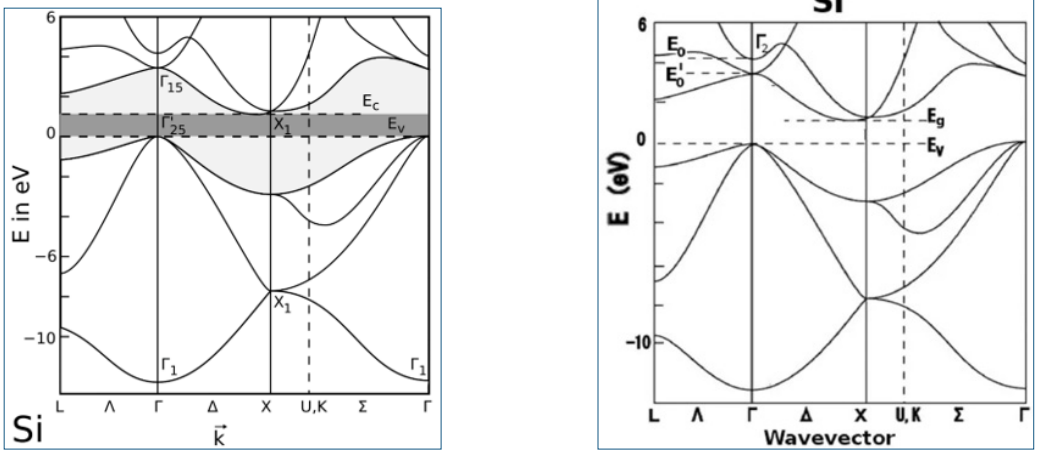

Figure 2: (a) Left-hand diagram: Si band structure showing energy vs wavevector in k-space. Seen are its variation between different symmetry points in k-space. (b) right-hand diagram: Electronic band diagram of silicon. It includes the L, Λ, Γ, Δ, X, U, K, and Σ symmetry points in the reciprocal space. E_0', E_0 and E_g are the two direct and the indirect band gaps, respectively, and E_v indicates the top of the valence band. See for (b) Nicolas Large, PhD thesis, Universite de Toulouse & Universidad del Pais Vasco, Oct. 11, 2011 [3].

where the ground state energy of the electron will reside. Lowest points of the conduction bands are located in the {100} directions along the X symmetry points, which can be approximated to be ellipsoids of revolution close to the conduction band minima. There are 6 of them, associated with the [±1, 0, 0], [0, ±1, 0] and [0, 0, ±1] directions. They are located 80 – 85 % of the way to the Brillouin boundary. Silicon is the workhorse of the transistor world for regular electronics. It is behind the integrated circuits used in much of the electronics used in radios, TV's, cell phones, and computers. The physics of the energy loss in silicon MOSFET type of devices was studies years ago [4-10]. The relatively small bandgap of silicon, and the fact that its bandgaps, although indirect, are located on the orthogonal axes, unlike germanium, which are on the {±1,±1,±1} family of axes, made it an ideal semiconductor with a small bandgap allowing for readily making transistor action possible. Germanium Ge has four equivalent conduction band ellipsoids valleys located at the edge of the Brillouin zone, along the {±1,±1,±1}directions. While there are eight half-ellipsoids at the zone boundary, because 2×2×2=8, they represent only a net total of four equivalent ellipsoids in k-space.

As indicated before, GaAs (also InP) became popular for RF electronics because of its improved performance for electron transport, as evidenced by its better electron effective masses, as well as its highly favorable direct bandgap property, indicated earlier [11-25]. Electron effective masses for silicon and germanium, relative to the free space electron mass m_0, are $m^*_{e,Si}/m_{e0}$ = 0.26 and $m^*_{e,Ge}/m_0$ = 0.12. Compare this to that of GaAs, which has $m^*_{e,GaAs}/m_{e0}$ = 0.067 . Therefore, GaAs has an improvement advantage over, respectively, silicon and germanium of 3.88 and 1.79, or nearly factors of four and two. Note that because both Si and Ge consist of multiple ellipsoidal valleys, the quoted elective masses values are really averages of the two characteristic effective masses for these ellipsoids. For Si, there are two transverse effective masses (determined by the two orthogonal coordinates of the cigar shaped thinner cross-section), and one longitudinal effective mass, given by, respectively, $m^*_{\perp e,Si}/m_{e0}$ = 0.19 and $m^*_{||e,Si}/m_{e0}$ = 0.19. Furthermore, when using holes for transport, there are not the improvements seen for GaAs versus either Si or Ge. In fact, the hole effective masses are $m^*_{h,GaAs}/m_{e0}$ = 0.31, $m^*_{h,Si}/m_{e0}$ = 0.36-0.39, $m^*_{h,Ge}/m_{e0}$ = 0.21. To further complicate the issues, holes are found in light and heavy hole valence bands. These specific values are given as $m^*_{hh,GaAs}/m_{e0}$ = 0.51, $m^*_{lh,GaAs}/m_{e0}$=0.082 for GaAs, $m^*_{hh,Si}/m_{e0}$ = 0.49 to 0.54, $m^*_{lh,Si}/m_{e0}$ = 0.155 for Si, and $m^*_{hh,Ge}/m_{e0}$ = 0.28 to 0.46 , $m^*_{lh,Ge}/m_{e0}$ = 0.043 to 0.16 . Range of values is due to curvature of band structure surface with effective masses calculated as the second derivative in $m^*_{ij} = \hbar^2\left[\frac{\partial^2 E(\mathbf{k})}{\partial k_i \partial k_j}\right]^{-1}$, where the *i, j* are selected to be coordinates in either the ellipsoidal local system, or say a rectilinear system *i, j*= x, y, z.

Possible Elements for SC: Informed by High Power Electronics and Examination of Their Semiconductor Band Structures

So, having just examined the transport semiconductor band structures and their transport carriers, one still speculates which elements might assist in raising the critical temperature for superconductors. On to the scene, comes two very interesting semiconductors, used in high power RF electronics. These semiconductors are GaN and SiC. Let's take a look at their band structures. Take a look at a sketch of the GaN band structure in Figure 3 [26], and a more detailed band structure diagram in Figure 4 [27].

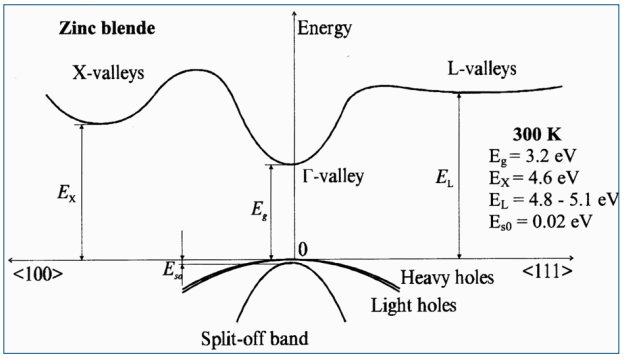

Figure 3: Band structure of zinc blende(cubic) GaN. Important minima of the conduction band and maxima of the valence band. 300K; E_g =3.2 eV; E_X= 4.6 eV; E_L = 4.8-5.1 eV; E_{so} = 0.02 eV. See Suzuki, M, T. Uenoyama, A. Yanase, First-principles calculations of effective-mass parameters of AlN and GaN, Phys. Rev. B 52, 11 (1995), 8132-8139 [26].

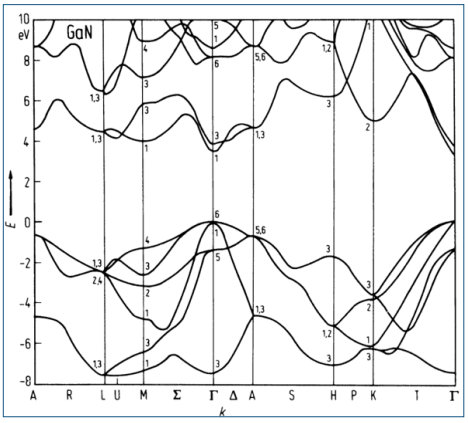

Figure 4: GaN, Wurtzite. Band structure calculated with an empirical pseudopotential method. The band structure differs only slightly from other spin-neglecting calculations. Introduction of spin-orbit interaction leads to a splitting of the uppermost valence band at Γ from Γ1 + Γ6 , into Γ9 + Γ7 + Γ7 . The energy differences between these terms can be described by two parameters - the spin-orbit splitting energy E_{so} (Δ_{so}) and the crystal field splitting energy E_{cr}(Δ_{cr}); see Bloom, S., Harbeke G., Meier E., Ortenburger I.B., "Band Structure and Reflectivity of GaN", Phys. Stat. Solidi 66, 161-168, 1974 [27].

One sees from Figures 3 and 4 that the bandgap for GaN is E_g^{GaN} = 3.2 eV. This is considerably bigger, by a factor of E_g^{GaN}/E_g^{GaAs} = 3.2/1.42 = 2.25 than GaAs. This gives GaN electronics, especially transistors, a distinct advantage of being less disrupted by higher temperature thermal noise, which also can include overheating compared to electronics utilizing GaAs. Although, in GaAs, Ga is a metal and As a metaloid, GaN is a combination of a Ga metal and a nonmetal. This makes the compound GaN distinctly different than GaAs. This points the way toward replacing the oxygen backbones seen in cuprate superconductors with nitrogen. The advantage in obtaining much higher operating temperatures for electronics utilizing the nonmetal element N in GaN, may very will help in elevating superconducting critical temperatures T_C . This also points the way too having more compatible chemistries between superconducting materials and electronics if one ever envisions integrated circuits using high T_C SC materials.

Following this line of reasoning, one can ask if there are other understood high power electronics employing nonmetal atoms. The answer is a resounding yes, in the compound semiconductor material SiC. Figure 5 shows the band structure of 4-H SiC,

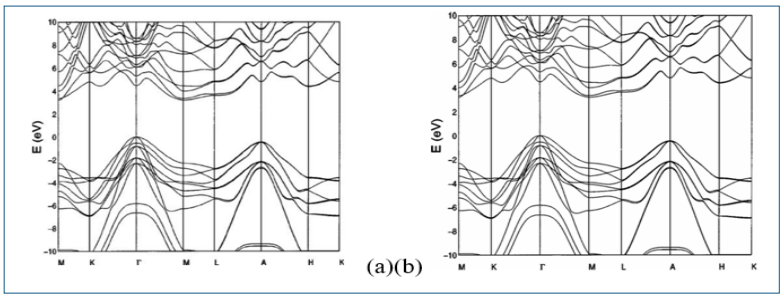

Figure 5: (a), The Band structure of 4-H SiC; (b), the Band structure of 6-H SiC, See G. Pennington, N. Goldsman, "Self-Consistent Calculations for n-type Hexagonal SiC Inversion Layers," J. Appl. Phys. 95 (8), 4223 – 4234,15 April 2004 [28].

and 6-H SiC.

Bandgap for SiC for three types of SiC, namely, 3C-SiC, 4H-SiC, and 6H-SiC, are respectively, $E_g^{(3C\text{-}SiC)} = 2.3$ eV, $E_g^{(4H\text{-}SiC)} = 3.2$ eV, and $E_g^{(4H\text{-}SiC)} = 3.0$ eV [29].

These bandgaps make SiC suitable for high-temperature, radiation-resistant, and high-speed electronic applications. The wide b and gap allows SiC to operate at temperatures exceeding 200°C without significant degradation, making it a preferred choice for industries seeking durable, high-performance solutions. SiC has these many polymorphs, typical of compound materials. In fact, 250 are known, with some lattice constants 301.5 nm, a thousand times larger than the usual lattice spacings [30]. But usually only a few are utilized for electronics. The polymorphs of SiC include a large group of similar crystalline structures called polytypes, which are manifestations of the same compound in 2D but differ in the third dimension [31]. This allows them to be viewed as layers stacked in a particular order, and arranged in three configurations, labeled A, B, or C, to achieve the closest packing. Each unique sequence constitutes a unit crystal cell.

Figure 6 shows the 2H-SiC, 4H-SiC and 6H-SiC polytypes. Note that the 6H-SiC polytypes are the most easily prepared by growth techniques. The nomenclature is the Ramsdell notation, here the "H" stands for hexagonal, where the number indicates the layer and the letter indicate the Bravais lattice type [32]. The 2H-SiC structure is equivalent to that of wurtzite and is composed of only elements A and B stacked as ABABAB. The 4H-SiC unit cell is two times longer, and the second half is twisted compared to 2H-SiC, resulting in ABCB stacking. The 6H-SiC cell is three times longer than that of 2H, and the stacking sequence is ABCACB. The cubic 3C-SiC, also called β-SiC, has ABC stacking.

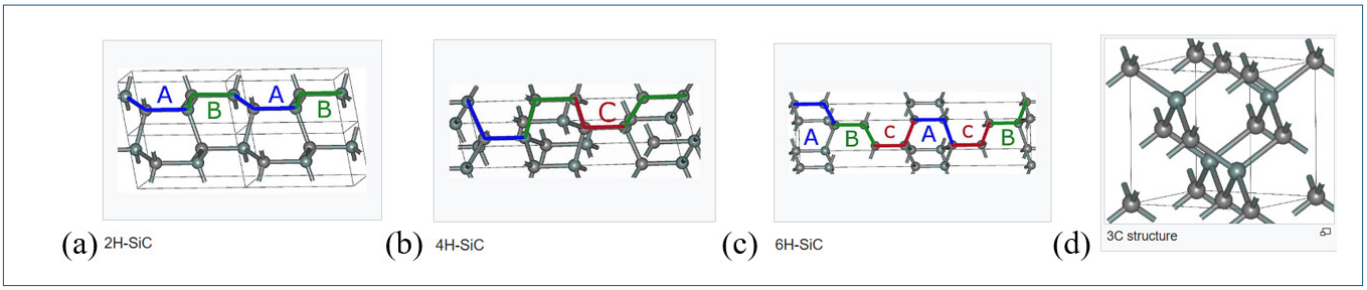

Figure 6: Crystal Stuctures of the (a) 2H-SiC, (b) 4H-SiC, (c) 6H-SiC, (d) 3C-SiC polytypes.

Atomic Substitution of Oxygen with Either N or C

Now that we have learned something about the amazing properties of the high-power electronic RF transistors employing either the element N in Ga nor C in SiC, one is very encouraged to replace O atoms in the oxygen backbone of cuprate superconductors with these nonmetallic elements. Let's do this for a few representative unit cell cuprate crystal structures. Before going ahead with this plan, it would be good to review some of the essential characteristics of the atoms involved. Because one is replacing oxygen O atoms, look up some of their properties. Electron orbital configuration is $[He]2s^22p^4$, with main valence state -2, with four other less common valence states of -1, 0, +1, +2. Oxygen has $N_p = 8$ protons in its nucleus, and $N_n = 8$ neutrons in its nucleus, giving its atomic weight as $A_w = N_p + N_n = 8 + 8 = 16$. Its atomic number is given as $N_A = N_p = 8$. One can denote in shorthand oxygen as $^{16}O_8$. Nitrogen which is to replace it, another nonmetallic element, has an electron orbital configuration of $[He]2s^22p^3$, atomic number of $N_A = 7$, and an atomic weight of $A_w = 14$, giving a shorthand notation of $^{14}N_7$. Common valence states for nitrogen are -3, +3, +5, with six other less common valence states of -2, -1, 0, +1, +2, +4. The third nonmetallic being considered to replace oxygen is carbon C. It has an electron orbital configuration of $[He]2s^22p^2$, atomic number of $N_A = 6$, and an atomic weight of $A_w = 12$, giving a shorthand notation of $^{12}C_6$. Carbon has many common valence states, including -4, -3, -2, -1, 0, +1, +2, +3, +4.

Since one is swapping out O with either N or C atoms, it will be useful to discuss their respective atomic or covalent radaii. For oxygen, one has $r_{cov}^{O} = 0.066$ Å . For nitrogen, the value is somewhat larger, with a value of $r_{cov}^{N} = 0.071$ Å . Carbon has somewhat a different situation since its s and p orbitals hybridize into 3D-, 2D-, and 1D-like orbital arrangements, denoted as sp^3, sp^2, and sp forms. Their respective radaii are are $r_{cov;\,sp^3}^{C} = 0.077$ Å , $r_{cov;\,sp^2}^{C} = 0.073$ Å , and $r_{cov;\,sp}^{C} = 0.069$ Å . So the swapping out radaii ratios between oxygen and the two other elements nitrogen and carbon are given by

$$\frac{r_{cov}^{N} - r_{cov}^{O}}{r_{cov}^{O}} = \frac{(0.071 - 0.066)\,\text{Å}}{0.066\,\text{Å}} = 0.0758 \tag{1}$$

The result for swapping out O with C atoms is a bit more nuanced, due to the various possible dimensional orbital hybridization configurations. The calculations go as follows.

$$\frac{r_{cov}^{C} - r_{cov}^{O}}{r_{cov}^{O}} = \frac{(77, 73, 69)^{3D,2D,1D} \times 10^{-3}\,\text{Å}}{0.066\,\text{Å}} = 0.167, .0106, 0.046 \tag{2}$$

Now look at some unit cell cuprate crystal structures, in Figure 7. Cuprate materials are what led the research community into the very high critical temperature realm. There are the Hg mercury based compounds like Hg-1223 $HgBa_2Ca_2Cu_3O_{8+\delta}$ with a $T_C = 134$ K and the simpler sister compound which is a Hg-1212 $HgBa_2CaCu_2O_{6+\delta}$ with a $T_C = 104$ K (with one less Cu plane, also reducing the Ca and Cu counts by one each) but with extra annealing T_C rise to 123 K, the Tl thallium based compounds like Tl-2223 $TlBa_2Ca_2Cu_3O_{10}$ with a $T_C = 125$ K, mixed Hg and Tl compounds which is still a (Tl, Hg)-2223 form with a (Tl1.6Hg0.4) with a T_C

= 130 K, bismuth Bi based compounds like $Bi_2Sr_2Ca_2Cu_3O_{10}$ which is a Bi-2223 with a T_C = 110 K, and rare-earth based compounds like $YBa_2Cu_3O_7$ denoted YBCO with a T_C = 92 K. For $HgBa_2Ca_2Cu_3O_{8+\delta}$, its crystal structure is shown in Figure 7 (a) [33-34].

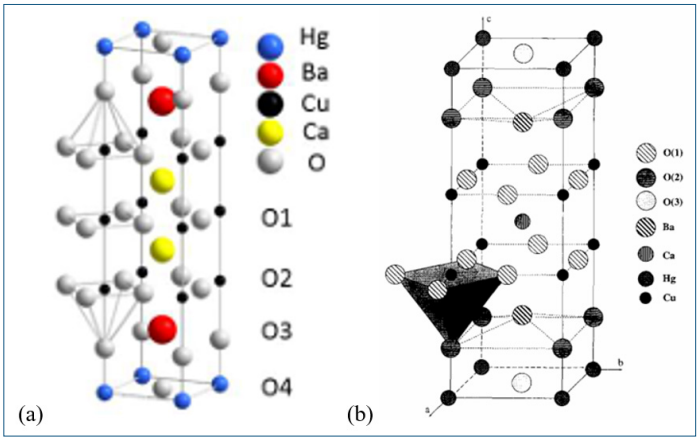

Figure 7: (a) Crystal structure of the cuprate superconductor $HgBa_2Ca_2Cu_3O_{8+\delta}$ unit cell [33-34]. Note that placement of an O atom on each end face is technically not correct as one of those atoms must be missing to obtain a partial shortage of an O atom to yield a δ fractional contribution. (b) Crystal structure of the cuprate superconductor $HgBa_2CaCu_2O_{6+\delta}$ unit cell [35].

The simpler sister compound $HgBa_2CaCu_2O_{6+\delta}$ has the symmetry of space group P4/mmm and lattice parameters a = 3.8526 (2) Å, c = 12.6367(8) Å with δ=0.35, but with further annealing δ is lowered to δ = 0.28 and T_C raised by19 K [35]. Other related studies are for $Hg_{1-x}Pb_xBa_2Ca_2Cu_3O_y$ [36] (Figure 7 (b)). The composition of this sample has been found experimentally and is specified by a formula of $Hg_{0.66}Pb_{0.34}Ba_2Ca_{1.98}Cu_{2.30}O_{8.4}$. Still another variant has a Tl substitution, $Hg_{0.8}T_{l0.2}Ba_2Ca_2Cu_3O_{8+\delta}$, with the compound having the same crystal as Hg-1223 with the space group symmetry P4/mmm and lattice parameters a = 3.8489(1) Å, c = 15.816(1) Å [37]. Rietveld analysis results indicate that Hg is partially replaced by Tl, and the oxygen content, δ, is 0.33, with a T_C = 138 K. Let us do the replacement of oxygen with nitrogen in Figure 7 (a) in $HgBa_2Ca_2Cu_3O_{8+\delta}$ by making the O atoms go into N atoms, obtaining Figure. 8 (a). Doing this also for the sister superconductor $HgBa_2CaCu_2O_{6+\delta}$ gives us $HgBa_2CaCu_2N_{6+\delta}$ in Figure. 8 (b).

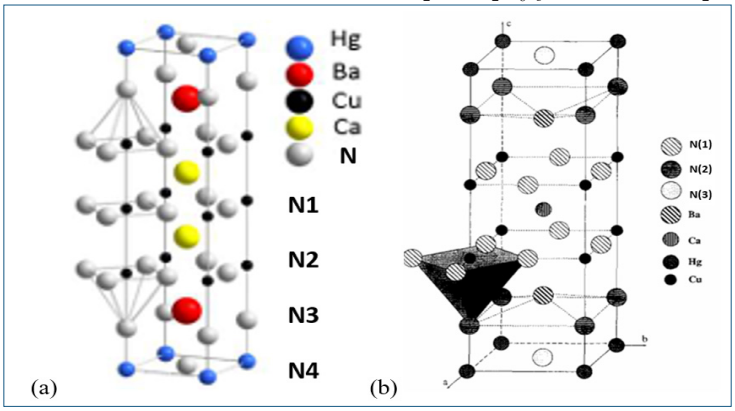

Figure 8: (a) Crystal structure of the cuprate superconductor $HgBa_2Ca_2Cu_3N_{8+\delta}$ unit cell [33], [34]. Note that placement of an N atom on each end face is technically not correct as one of those atoms must be missing to obtain a partial shortage of an N atom to yield a δ fractional contribution. (b) Crystal structure of the cuprate superconductor $HgBa_2CaCu_2N_{6+\delta}$ unit cell. Same comment here for end face N atoms applies as in (a) that to obtain a partial shortage of an N atom to yield a δ fractional contribution, not all end faces have an N atom [35].

Let us do the replacement of oxygen with carbon in Figure 7 (a) in $HgBa_2Ca_2Cu_3O_{8+\delta}$ by making the O atoms go into C atoms, obtaining $HgBa_2Ca_2Cu_3C_{8+\delta}$ in Figure 9 (a). Doing this also for the sister superconductor $HgBa_2CaCu_2O_{6+\delta}$ gives us $HgBa_2CaCu_2C_{6+\delta}$ in Figure 9 (b).

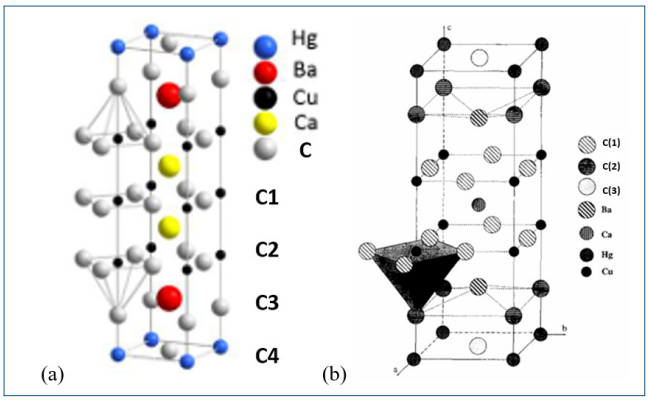

Figure 9: (a) Crystal structure of the cuprate superconductor $HgBa_2Ca_2Cu_3C_{8+\delta}$ unit cell [33,34]. Note that placement of an Catom on each end face is technically not correct as one of those atoms must be missing to obtain a partial shortage of an C atom to yield a δ fractional contribution. (b) Crystal structure of the cuprate superconductor $HgBa_2CaCu_2C_{6+\delta}$ unit cell. Same comment here for end face C atoms applies as in (a) that to obtain a partial shortage of an C atom to yield a δ fractional contribution, not all end faces have an C atom [35].

Substitutional Replacement of the Charge Sharing Atoms Interacting with the Conducting Tracks

Charge sharing atoms could include atoms such as barium Ba or calcium Ca. Barium has an electronic orbital configuration of [Xe] $6s^2$ with common valence states of +1and+2. Its atomic number is $N_A = 56$, and atomic weight is $A_w = 137$. Barium is somewhat unusual in having quite a number of stable isotopes. They are $^{130}Ba_{56}$, $^{132}Ba_{56}$, $^{134}Ba_{56}$, $^{135}Ba_{56}$, $^{136}Ba_{56}$, $^{137}Ba_{56}$, $^{138}Ba_{56}$, with percentage abundances, respectively of, 0.11 %, 0.1 %, 2.42 %, 6.59 %, 7.85 %, 11.2 %, and 71.7 %. Barium is an alkaline earth metal, with high chemical reactivity. Barium provides holes into the lattice of the cuprate $LaCuO_4$ converting it into $La_{2-x}Ba_x Cu_4$ when it substitutes for the trivalent cation La^{3+} with its divalent cation form Ba^{2+}. Difference between the ionization states is exactly (3+) – (2+) = 1+, resulting in a floating free "+" charge, and it is this free floating charge that provides the mobile hole, which gravitates to the copper conducting planes. These holes are used in the CuO_2 layers which conduct charges. For the rare earth superconductor YBCO $YBa_2Cu_3O_{7-x}$, the BaO layers act as charge reservoirs, transferring holes to the conducting copper CuO_2 planes. What the Ba atoms do is enable the parent insulating"Mott"state to change into a superconducting state. Note that its covalent radius is $r_{cov}^{Ba} = 0.215$ Å

What about calcium? It is also an alkaline earth metal. It is considerably lighter than barium, with an atomic number is $N_A = 20$, and atomic weight is $A_w = 40$. Like barium, it also has quite a number of stable isotopes, those being $^{40}Ca_{20}$, $^{42}Ca_{20}$, $^{43}Ca_{20}$, $^{44}Ca_{20}$, $^{46}Ca_{20}$, $^{48}Ca_{20}$, with abundances, respectively, of 96.9 %, 0.647 %, 0.135 %, 2.09 %, 0.004 %, 0.187 %, with the last isotope not stable but with a hugely long half-life exceeding 10^{19} years. Its electronic orbital configuration is [Ar] $4s^2$, with common valence states of states of +1 and +2. Although considerably lighter than barium, its orbital characteristic generates similar charge substitutional behavior. Its covalent radius is $r_{cov}^{Ca} = 0.176$ Å.

One can calculate the percentage difference between the barium and calcium atoms.

$$\frac{r_{cov}^{Ba} - r_{cov}^{Ca}}{\langle r_{cov}^{Ba,Ca} \rangle_{av}} = \frac{(0.215 - 0.176)\text{ Å}}{0.1955\text{ Å}} = 0.1995 \quad (3)$$

where

$$\langle r_{cov}^{Ba,Ca} \rangle_{av} = \frac{r_{cov}^{Ba} + r_{cov}^{Ca}}{2} \quad (4)$$

So, the question at hand is there an advantage to replacing either of these atoms with other element atoms that can deliver something more? One obvious response this this question is that perhaps another atom type can more easily provide a greater charge transfer other than the +1 advantage of say swapping out La with these lower common valence state atoms. To obtain a +2 advantage, one needs atoms with common easily obtainable valence states of +1. They may be found in Group 1 of the Periodic Table of Elements, including hydrogen H, lithium Li, sodium Na, potassium K, rubidium Rb, cesium Cs, and from Group 11, namely silver Ag and gold Au. All of these atoms possess a single valence electron in their outermost shell. Their electron orbital configurations are $H_{eoc} = 1s^1$, Li_{eoc} = [He] $2s^1$, Na_{eoc} = [Ne] $3s^1$, K_{eoc} = [Ar] $4s^1$, Rb_{eoc} = [Kr] $5s^1$, Cs_{eoc} = [Xe] $6s^1$ for the Group 1 elements, and Ag_{eoc} = [Kr] $4d^{10}$ $5s^1$, Au_{eoc} = [Xe] $4f^{14}$ $5d^{10}$ $6s^1$ for the Group 11 elements. Group 11 elements load up their d and f orbitals, before getting to their single occupied s orbital. Gold is particularly unreactive chemically because both its d and f orbitals are fully filled. The covalent radaii of the Group 1 elements are $r_{cov}^{H} = 0.031$ Å, $r_{cov}^{Li} = 0.128$ Å, $r_{cov}^{Na} = 0.166$ Å, $r_{cov}^{K} = 0.203$ Å, $r_{cov}^{Rb} = 0.220$ Å, $r_{cov}^{Cs} = 0.244$ Å, whereas Group 11 elements have $r_{cov}^{Ag} = 0.145$ Å, $r_{cov}^{Au} = 0.136$ Å.

What is needed is to find the covalent radaii differences between the present charge sharing atoms, Ba and Ca, and those to be swapped in their places. First look at switching out Ba with Group 1 elements.

$$\frac{r_{cov}^{\text{Group 1}} - r_{cov}^{\text{Ba}}}{r_{cov}^{\text{Ba}}} = \frac{[(128, 166, 203, 220, 244)^{Group\ 1} - 0.215] \times 10^{-3}\ \text{Å}}{0.215\ \text{Å}}$$

$$= -0.405, -0.228, -0.0558, 0.0233, 0.135 \quad (5)$$

Here we have excluded looking at hydrogen. The results are given for the Group 1 elements, from left-to-right for Li, Na, K, Rb, and Cs. For the Group 11 elements one has

$$\frac{r_{cov}^{\text{Group 11}} - r_{cov}^{\text{Ba}}}{r_{cov}^{\text{Ba}}} = \frac{[(145, 136)^{Group\ 11} - 0.215] \times 10^{-3}\ \text{Å}}{0.215\ \text{Å}}$$

$$= -0.326, -0.367 \quad (6)$$

Conclusion from inspecting the results in (5) and (6) is that to stay below a 15 % change in covalent radaii change, for the Group 1 elements, one must only use atoms K, Rb, or Cs. Use of Group 11 elements is precluded, as both Ag, and Au exceed 30%.

Next find the covalent radaii differences between the other charge sharing atom Ca, and those to be swapped in its place.

$$\frac{r_{cov}^{\text{Group 1}} - r_{cov}^{\text{Ca}}}{r_{cov}^{\text{Ca}}} = \frac{[(128, 166, 203, 220, 244)^{Group\ 1} - 0.176] \times 10^{-3}\ \text{Å}}{0.176\ \text{Å}}$$

$$= -0.273, -0.0568, 0.153, 0.250, 0.386 \quad (7)$$

Here again we have excluded looking at hydrogen. The results are given for the Group 1 elements, from left-to-right for Li, Na, K, Rb, and Cs. For the Group 11 elements one has

$$\frac{r_{cov}^{\text{Group 11}} - r_{cov}^{\text{Ca}}}{r_{cov}^{\text{Ca}}} = \frac{[(145, 136)^{Group\ 11} - 0.176] \times 10^{-3}\ \text{Å}}{0.176\ \text{Å}}$$

$$= -0.176, -0.227 \quad (8)$$

Inspecting the results in (7) and (8), in order is to stay below a 15 % change in covalent radaii change, for the Group 1 elements, one must only use atoms Na or K. Again, use of Group 11 elements is precluded, as both Ag, and Au exceed15 %, but the excess difference for Ag is only 2.6% too low.

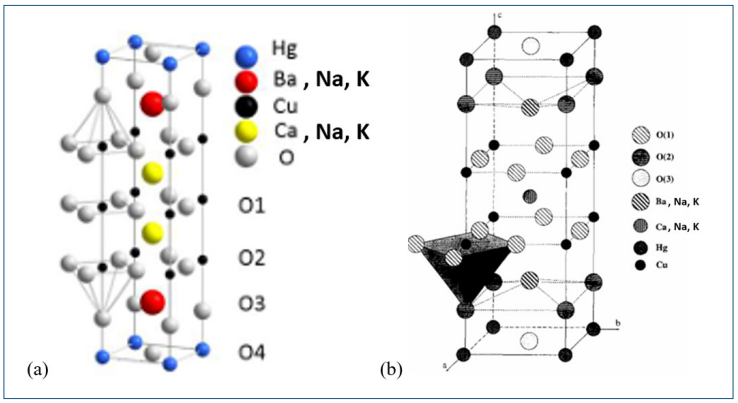

Figure 10: (a) Crystal structure of the modified charge sharing cuprate superconductor $HgBa_{2-x-y}Na_xK_yCa_{2-z-w}Na_zK_wCu_3C_{8+\delta}$ unit cell [33,34]. Note that placement of atoms Na or K on the charge sharing atoms Ba or Ca or both (b) Crystal structure of the modified charge sharing cuprate superconductor $HgBa_{2-x-y}Na_xK_yCa_{1-z-w}Na_zK_wCu_2C_{6+\delta}$ unit cell. Same comment here as in (a), note the placement of atoms Na or K on the charge sharing atoms Ba or Ca or both [35].

The thought that such replacements as indicated here are completely reasonable comes from examining a much lower high T_C superconductor class, the pnictides. For example, replacement atom doping to obtain carriers was seen for the pnictide $BaFe_2As_2$ with potassium doping K, becoming $(Ba_{1-x}K_x)\ Fe_2As_2$ [38,39]. Or for pnictide $SrFe_2As_2$ with K or cesium Cs doping, giving$(A_{1-x}Sr_x)\ Fe_2As_2$ with A=K and Cs [40,41].

Substitutional Replacement of the Conducting Track Atoms

Copper atoms constitute the conducting track atoms for cuprate superconductors. Copper is a very well known metal (in fact a transition metal) used in many integrated circuit applications, as well as being used in many conventional household items such as cables for kitchen (toasters, ovens, dishwashers), washing and drying machines, power strips, extension cords. Atomic number and weight for copper are $N_A = 29$, and an atomic weight of $A_w = 63$, giving a shorthand notation of $^{63}Cu_{29}$, with the number of protoins being $N_p = N_A$, and the number of neutrons $N_n = N_w - N_p = 34$. This isotope of copper, is the more common form, with an abundance

of 69.2 %. Its other stable isotope is $^{65}Cu_{29}$ with 2 extra neutrons in its nucleus, with an abundance of 30.9 %. Copper has an electron orbital configuration of $[Ar]3d^{10}4s^1$ and a common valence state of +2, with other less common valence states of -2, -1, 0, +1, +3, +4. Copper's covalent radius is $r_{cov}^{Cu} = 0.132$ Å . Its common valence state is +2, with other less common valence states of -2, -1, 0, +1, +3, +4. Clearly, its most common valency must result from a contributing $4s^1$ electron, as well as a single 3d electron. Loss of two electrons from theCuatom, yields Cu^{2+} ions in the lattice. One could only improve on this by inserting atoms with a higher positive valency.

Elements which exceed 2+ valency include Groups 3A, 4A, and 5A from the periodic table, as well as transition elements. For 3+ valency, there are Al^{3+}, Sc^{3+}, Ga^{3+}, Fe^{3+}, B^{3+}, V^{3+} and some of the lanthanides like La^{3+}. Note that boron B is a metalloid, not a metal, but scandium Sc and iron Fe are both transition metals, whereas aluminum Al and gallium Ga are both post-transition metals. For 4+ valency, there are C^{4+}, Si^{4+}, Sn^{4+}, Ti^{4+}, Mn^{4+}, V^{4+}. Here carbon C is a nonmetal and silicon Si is a metalloid, but titanium Ti, manganese Mn and vanadium V are all transition metals, whereas tin Sn is a post transition metal. For 5+ valency, N^{5+}, P^{5+}, V^{5+}, where both N and P are nonmetals, whereas vanadium V is a transition metal. For 6+ valency, Cr^{6+}. which is a transition metal. Vanadium is very special in that it has four commonly used ion valency states (V^{2+},V^{3+},V^{4+},V^{5+}) in all-vanadium redox flow battery (VRFBs) electrolytes.

If one realizes excluding nonmetals is desirable for a Cu replacement atom, and metalloids, and possibly excluding some post-transition metals, then our list of possibilities is narrowed down to a more realistic list to consider. A further narrowing may be useful at this point also in excluding also the lanthanide series of metals. Therefore, retain for consideration: Al^{3+}, Sc^{3+}, V^{3+} ; Ti^{4+}, Mn^{4+}, V^{4+}; V^{5+} ; Cr^{6+}. Let's investigate properties of these potential atom replacements. Aluminum has a single stable isotope, with $N_{p,\,Al} = 13$ and $N_{n,\,Al} = 14$, making $A_{w,\,Al} = 27$, with notation $^{27}Al_{13}$. Its electronic orbital configuration is [Ne] $3s^2\ 3p^1$, which demonstrates that to getthe +3ionic charged state, both the single electron in the 3p orbital, and the two electrons in the 3s orbital, must be released. Aluminum's electrical conductivity is $\sigma_{electr}^{Al} = 3.8\times10^7$ S/m. Compare this to copper which is $\sigma_{electr}^{Cu} = 5.96\times10^7$ S/m, or gold at $\sigma_{electr}^{Au} = 4.52\times10^7$ S/m, or silver with $\sigma_{electr}^{Ag} = 6.30\times10^7$ S/m, which has the highest value for any metal. Covalent radius for AI is $r_{cov}^{Al} = 0.121$ Å, but one should realize that removal of electrons reduces the atomic radius $r_{atomic}^{Al} = 0.143$ Å to $r_{4\text{-}coord}^{Al} = 0.039$ Å for a 4-coordinated atom in a lattice, and somewhat larger to $r_{6\text{-}coord}^{Al} = 0.053$ Å for a 6-coordinated atom in a lattice. Using the covalent radaii as some measure of replacement ability, as before, comparison of aluminum to copper yields

$$\frac{r_{cov}^{Al} - r_{cov}^{Cu}}{r_{cov}^{Cu}} = \frac{(0.121 - 0.132)\ Å}{0.132\ Å} = -0.0833 \tag{9}$$

What about the element scandium? It has only one stable isotope, $^{45}Sc_{21}$, with $N_{p,\,Sc} = 21$ protons and $N_{n,\,Sc} = 24$ neutrons, making its atomic weight $A_{w,\,Sc} = 45$. Its electronic orbital configuration is [Ar] $3d^1\ 4s^2$, which demonstrates that to get the +3 ionic charged state, both the single electron in the 3d orbital, and the two electrons in the 4s orbital, must be released. Scandium's electrical conductivity is $\sigma_{electr}^{Sc} = 1.85\times10^6$ S/m. Clearly, this is considerably lower than metals like Ag, Au, Al, and Cu, lower by a factor of a 10. Because 1 S = 1 Siemen = 1/Ohm = 1/Ω, restated in terms of inverse Ohms and cm, is $\sigma_{electr}^{Sc} = 1.85\times10^4$ 1/Ω·cm . As for its covalent radius, one finds $r_{cov}^{Sc} = 0.170$ Å . This differs from copper by

$$\frac{r_{cov}^{Sc} - r_{cov}^{Cu}}{r_{cov}^{Cu}} = \frac{(0.170 - 0.132)\ Å}{0.132\ Å} = 0.288 \tag{10}$$

making scandium considerably larger by nearly 30 % than copper, in terms of the covalent radius. Let's move on to vanadium, with an electronic orbital configuration of [Ar] $3d^3\ 4s^2$, and atomic number of $N_{p,\,V} = 23$, atomic weight of $A_{w,\,V} = 51$, and number of neutrons $N_{n,\,V} = 28$. There is only one stable isotope of vanadium. Vanadium can take on various ionic charges, from +2, +3, +4, and +5 as in the vanadium redox flow battery electrolyte, showing that this clearly arises by the loss of two electrons from the 4s orbital for the +2 charge state, and successively more electrons from the 3d orbital, to obtain the three other higher ionic states. Its covalent radius is $r_{cov}^{V} = 0.153$ Å . Let's compare this to copper,

$$\frac{r_{cov}^{V} - r_{cov}^{Cu}}{r_{cov}^{Cu}} = \frac{(0.153 - 0.132)\ Å}{0.132\ Å} = 0.159 \tag{11}$$

significantly larger than copper. Electrical conductivity of vanadium metal is $\sigma_{electr}^{V} = 5.20\times10^6$ S/m, which is an order of magnitude below the most conducting metals. Titanium is another interesting metal, with an electronic orbital configuration of [Ar] $3d^2\ 4s^2$, and atomic number of $N_{p,\,V} = 22$, atomic weight of $A_{w,\,V} = 48$, and number of neutrons $N_{n,\,V} = 26$. There are several titanium isotopes, being $^{46}Ti_{22}$, $^{47}Ti_{22}$, $^{48}Ti_{22}$, $^{49}Ti_{22}$, and $^{50}Ti_{22}$, with abundances, respectively, of 8.25 %, 7.44 %, 73.7 %, 5.41 %, 5.18 % . The +4 valance state of titanium occurs when the 4s orbital loses both of its electrons, as well as the 3d orbital loosing both of its electrons. Its covalent radius is $r_{cov}^{Ti} = 0.160$ Å . Let's compare this to copper,

$$\frac{r_{cov}^{Ti} - r_{cov}^{Cu}}{r_{cov}^{Cu}} = \frac{(0.160 - 0.132)\ Å}{0.132\ Å} = 0.212 \tag{12}$$

which is significantly larger than copper. Electrical conductivity of titanium metal is $\sigma_{electr}^{Ti} = 1.276\times10^6$ S/m, which is over an order of magnitude below the most conducting metals. Compared to copper,

$$\frac{\sigma_{electr}^{Ti}}{\sigma_{electr}^{Cu}} = \frac{1.276\times10^6\ S/m}{5.96\times10^7\ S/m} = 2.14\times10^{-2} \tag{13}$$

This makes titanium 42 times worse a conductor than copper. Obviously, it is instructive to go on to another possible metal, namely, manganeseMn. Electrical conductivity of manganese metal is $\sigma_{electr}^{Mn} = 6.2\times10^5$ S/m, which is an even worse conductor that titanium. Compared to copper,

$$\frac{\sigma_{electr}^{Mn}}{\sigma_{electr}^{Cu}} = \frac{6.2\times10^5\ S/m}{5.96\times10^7\ S/m} = 1.04\times10^{-2} \tag{14}$$

This makes manganese 84 times worse a conductor than copper, and twice as bad as titanium. It has an electronic orbital configuration of [Ar] $3d^5\ 4s^2$, and atomic number of $N_{p,\,Mn} = 25$, atomic weight of $A_{w,\,Mn} = 55$, and number of neutrons $N_{n,\,Mn} = 30$. There is only a single stable manganese isotope, being $^{55}Mn_{25}$. The +4 valance state of manganese occurs when the 4s orbital loses both of its electrons, and the 3d orbital looses two of its electrons, leaving it with $3d^3$. Most common oxidation states of manganese are +2, +4, and +7, although all oxidation states from −3 to +7 have been observed. Its covalent radius is seen in two spin states of high and low spin, given by $r_{cov,low\ spin}^{Mn} = 0.139$ Å and $r_{cov,high\ spin}^{Mn} = 0.161$ Å . Let's compare this to copper,

$$\frac{r_{cov,low/high}^{Mn} - r_{cov}^{Cu}}{r_{cov}^{Cu}} = \frac{(0.139/0.161 - 0.132)\ \text{Å}}{0.132\ \text{Å}} = 0.0530, 0.220 \tag{15}$$

Low spin Mn case is only about 5 % different from copper, whereas the high spin case is over 20 %.

Last atom to consider is chromium Cr, with common oxidation states of +3 and +6. Less common are the valence states of -4 to +5, excluding -3 state. Chromium has an electronic orbital configuration of [Ar] $3d^5\ 4s^1$, and atomic number of $N_{p,\,Cr} = 24$, atomic weight of $A_{w,\,Cr} = 52$, and number of neutrons $N_{n,\,Cr} = 28$. Chromium has four stable isotopes, $^{50}Cr_{24}$, $^{52}Cr_{24}$, $^{53}Cr_{24}$, $^{54}Cr_{24}$, with abundances, respectively, of 4.34 %, 83.8 %, 9.50 %, and 2.37 %. It is easy to see how the valence state of +6 arises, by losing its single 4s orbital electron, and its five 3d electrons, yielding a +6 state. Chromium has a covalent radius of $r_{cov}^{Cr} = 0.139$ Å . Compared to copper,

$$\frac{r_{cov}^{Cr} - r_{cov}^{Cu}}{r_{cov}^{Cu}} = \frac{(0.139 - 0.132)\ \text{Å}}{0.132\ \text{Å}} = 0.0530 \tag{16}$$

Electrical conductivity of chromium metal is $\sigma_{electr}^{Cr} = 1.276\times10^6$ S/m, which is over an order of magnitude below the most conducting metals. Compared to copper,

$$\frac{\sigma_{electr}^{Cr}}{\sigma_{electr}^{Cu}} = \frac{7.9\times10^6\ S/m}{5.96\times10^7\ S/m} = 1.33\times10^{-1} \tag{17}$$

This makes chromium only 7.2 times worse a conductor than copper. To put this in context with a few other metals, here are listed those at or over 10^7 S/m : $\sigma_{electr}^{Li} = 1.1\times10^7$ S/m, $\sigma_{electr}^{Be} = 2.5\times10^7$ S/m, $\sigma_{electr}^{Na} = 2.1\times10^7$ S/m, $\sigma_{electr}^{Mg} = 2.3\times10^7$ S/m, $\sigma_{electr}^{K} = 1.4\times10^7$ S/m, $\sigma_{electr}^{Ca} = 2.9\times10^7$ S/m, $\sigma_{electr}^{Fe} = 1.0\times10^7$ S/m, $\sigma_{electr}^{Co} = 1.7\times10^7$ S/m, $\sigma_{electr}^{Ni} = 1.4\times10^7$ S/m, $\sigma_{electr}^{Zn} = 1.7\times10^7$ S/m, $\sigma_{electr}^{Mo} = 2.0\times10^7$ S/m, $\sigma_{electr}^{Ru} = 1.4\times10^7$ S/m, $\sigma_{electr}^{Rh} = 2.3\times10^7$ S/m, $\sigma_{electr}^{Pd} = 1.0\times10^7$ S/m, $\sigma_{electr}^{Cd} = 1.4\times10^7$ S/m, $\sigma_{electr}^{In} = 1.2\times10^7$ S/m, $\sigma_{electr}^{W} = 2.0\times10^7$ S/m, $\sigma_{electr}^{Os} = 1.2\times10^7$ S/m, $\sigma_{electr}^{Ir} = 2.1\times10^7$ S/m. Ones sees there are quite a few of them with substantial conductivities.

In these fairly conductive metals, rhodium is rare, and would be too costly to employ, although its electrical conductivity is somewhat better than being a third of copper.

$$\frac{\sigma_{electr}^{Rh}}{\sigma_{electr}^{Cu}} = \frac{2.3\times10^7\ S/m}{5.96\times10^7\ S/m} = 0.386 \tag{18}$$

Its covalent radius is $r_{cov}^{Rh} = 0.142$ Å. Rhodium has only one stable isotope, $^{103}Rh_{45}$, so one sees it is a fairly heavy element, with an electron orbital configuration of [Kr] $4d^8\ 5s^1$, allowing it to have a common valence state of +3. This common valency makes it an intriguing possibility, although still unlikely to be realistically used. One suspects from its orbital configuration, that it would have many other possible valence states, and this is the case, as electrons are released from its 4d orbital. Moving on to a much more available element, consider beryllium. It is a divalent atom like copper, thus has a common valence state of +2, and has an electronic orbital configuration of [He] $2s^2$, and atomic number of $N_{p,\,Be} = 4$, atomic weight of $A_{w,\,Be} = 9$, and number of neutrons $N_{n,\,Be} = 5$. It is an alkaline earth metal, with a covalent radius of $r_{cov}^{Be} = 0.096$ Å. Beryllium is also quite rare, constituting just 4×10^{-4} % by mass of the earth's crust. There is only one stable isotope of beryllium, $^{9}Be_4$. However, its electrical conductivity is quite respectable, at $\sigma_{electr}^{Be} = 2.5\times10^7$ S/m, comparing favorably to copper, at over 40 % of it,

$$\frac{\sigma_{electr}^{Be}}{\sigma_{electr}^{Cu}} = \frac{2.5\times10^7\ S/m}{5.96\times10^7\ S/m} = 0.420 \tag{19}$$

Magnesium may be another possibility, as its electrical conductivity at $\sigma_{electr}^{Mg} = 2.3\times10^7$ S/m, and compares quite well also to copper,

$$\frac{\sigma_{electr}^{Mg}}{\sigma_{electr}^{Cu}} = \frac{2.3\times10^7\ S/m}{5.96\times10^7\ S/m} = 0.386 \tag{20}$$

which is what one had for rhodium, which one decided is unacceptable as a practical element to extract and produce. Like beryllium, magnesium is an alkaline earth metal, and is still relatively light with an electronic orbital configuration of [Ne] $3s^2$, and atomic number of $N_{p,\,Mg} = 12$, atomic weight of $A_{w,\,Mg} = 24$, and number of neutrons $N_{n,\,Mg} = 12$. Not surprisingly, its common valence state is +2. This is then no better than copper. Magnesium is an abundant element at 13 % of earth's mass, so at least its extraction and use would not be an issue. Its covalent radius is $r_{cov}^{Mg} = 0.096$ Å.

Another element only slightly worse in conductivity than magnesium is molybdenum, with $\sigma_{electr}^{Mo} = 2.0\times10^7$ S/m. Molybdenum is a transition element metal, and has a moderate weight with an electronic orbital configuration of [Kr] $4d^5\ 5s^1$, and atomic number of $N_{p,Mo} = 42$, atomic weight of $A_{w,Mo} = 96$, and number of neutrons $N_{n,Mo} = 50$ - 58. Molybdenum has six stable isotopes, $^{92}Mo_{42}$, $^{94}Mo_{42}$, $^{95}Mo_{42}$, $^{96}Mo_{42}$, $^{97}Mo_{42}$, $^{98}Mo_{42}$, and $^{100}Mo_{42}$ with a half-life of 7.07×10^{18} years, with abundances, respectively, of 14.7 %, 9.19 %, 15.9 %, 16.7 %, 9.58 % , 24.3 % , and 9.74 %. Its common valence states are +4 and +6, which makes it a very interesting replacement atom for copper. It can also take on less common valence states of -4, -2, -1, 0, +1, +2, +3, +5, making molybdenum an ionically versatile atom. Quite obviously, if Mo takes on a valence state of +4, that provides a charge advantage over copper of two 2e. If Mo takes on the +6 valence state, charge advantage over copper of four 4e, which is impressive! Its covalent radius is $r_{cov}^{Mo} = 0.154$ Å. Compared to copper, one finds

$$\frac{r_{cov}^{Mo} - r_{cov}^{Cu}}{r_{cov}^{Cu}} = \frac{(0.154 - 0.132)\ \text{Å}}{0.132\ \text{Å}} = 0.167 \tag{21}$$

With the same conductivity as Mo, is tungsten (wolfram)W, at a value also at $\sigma_{electr}^{W} = 2.0\times10^7$ S/m. Its electronic orbital configuration is [Xe] $4f^{14}\ 5d^4\ 6s^2$, with common valence states of +4, +6. These ionic states are entirely consistent with its having two 6s electrons, and four 5d electrons. It also has a range of less common valence states of -4, -2, -1, 0, +1, +2, +3, +5. Tungsten has a covalent radius of $r_{cov}^{W} = 0.162$ Å,

$$\frac{r_{cov}^{W} - r_{cov}^{Cu}}{r_{cov}^{Cu}} = \frac{(0.162 - 0.132)\ \text{Å}}{0.132\ \text{Å}} = 0.227 \tag{22}$$

making it substantially bigger than copper. Tungsten is also considerably heavier then copper, with atomic number of $N_{p,W} = 74$, atomic weights of $A_{w,W} = 180$ - 186, and number of neutrons $N_{n,W} = 106$ - 112. Tungsten has four stable isotopes, $^{182}W_{74}$, $^{183}W_{74}$, $^{184}W_{74}$, $^{186}W_{74}$, and $^{180}W_{74}$ with a half-life of 1.59×10^{18} years, with abundances, respectively, of 26.5 %, 14.3 %, 30.6 %, 28.4 %, and 0.120 %. Tungsten is very attractive as a substitute for copper because of its potential high valency available states.

Having examined many possible replacements for the cuprate copper atom, a conducting track atom, one is left with only a few realistic possibilities that are not too much in varying from the copper covalent radius, exceed its valence state, and have as metals reasonably large electrical conductivities. The short list only includes molybdenum Mo , and tungsten W. If one insists on including atoms with identical common valencies, with acceptable radaii and electrical conductivities, then one could add into the possible atom's magnesium Mg, beryllium Be, and lastly the remote but still possible rhodium Rh. This last comment for rhodium arises because although it could be terribly costly to use in production, as a test element to try out new ideas, it could be ideal. Rhodium has a higher valency than copper, making it attractive to consider. If one does worry about either cost or rarity, the there are three atoms to choose from with valencies exceeding copper: Mo, W, and Rh. Figure 11 shows this final selection to try out.

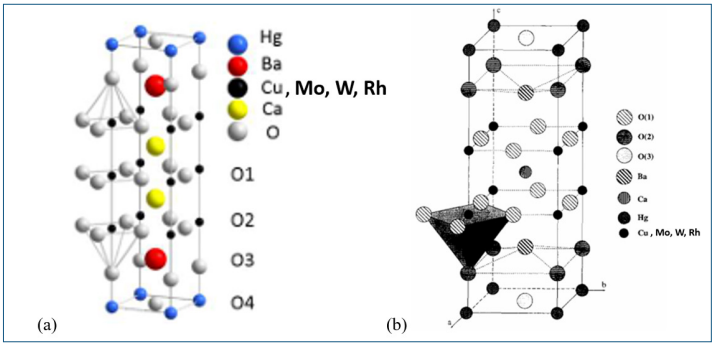

Figure 11: (a) Crystal structure of the cuprate superconductor unit cell $HgBa_2Ca_2Cu_{3-x-y-z}Mo_xW_y\ Rh_zO_{8+\delta}$ [33,34]. Note that placement of various possible atoms on the conducting track atom location. (b) Crystal structure of the cuprate superconductor $HgBa_2CaCu_{2-x-y-z}Mo_xW_yRh_zO_{6+\delta}$ unit cell [35]. Note that placement of various possible atoms on the conducting track atom location.

All of the efforts in trying to get at even higher critical temperatures suggests to us that one should turn some attention to how examining how T_C depends on the energy exchange mechanisms between the Cooper electrons and the possible sources of energy, be that phonons, space charge waves, spin waves, plasma motions, or any other mechanism that may arise.

Examination of the Critical Temperature from the Cooper Instability Equation

First one should look at the ladder superconducting Cooper vertex with disorder incorporated [42], [43]. Superconducting vertex Λ is a ladder sum of the total effective interaction , which includes the renormalized electron-electron, mediated phonon, and impurity scattering effects,

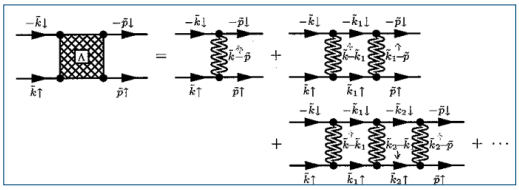

(23)

where $V_{eff,\,tot}^{RPA}$ is the total interaction due to these effects. Equation (23) can be restated as a Dyson type equation

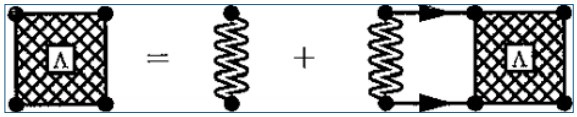

(24)

This vertex Dyson type equation, may be written out explicitly in terms of its vertex functions, quantum Green's functions, and effective total potential energy $V_{eff,\,tot}^{RPA}$:

$$\Lambda(\tilde{k},\,\tilde{p}) = -\,V_{eff\;tot}^{RPA}(\tilde{k}-\tilde{p}) \;+\; \frac{1}{\boldsymbol{\mathcal{V}}\beta}\sum_{\tilde{q},\,\lambda_{ph}}\Big[-\,V_{eff\;tot}^{RPA}(\tilde{k}-\tilde{q})\Big]G_{\uparrow}^{0}(\tilde{q})G_{\downarrow}^{0}(-\tilde{q})\Lambda(\tilde{q},\,\tilde{p}) \tag{25}$$

Noting that $V_{eff,\,tot}^{RPA} < 0$, writing it as $V' = -\,V_{eff,\,tot}^{RPA}$, and dropping the super- and sub- scripts for brevity,

$$\Lambda(\tilde{k},\,\tilde{p}) = V'(\tilde{k}-\tilde{p}) \;+\; \frac{1}{\boldsymbol{\mathcal{V}}\beta}\sum_{\tilde{q},\,\lambda_{ph}}\Big[V'(\tilde{k}-\tilde{q})\Big]G_{\uparrow}^{0}(\tilde{q})G_{\downarrow}^{0}(-\tilde{q})\Lambda(\tilde{q},\,\tilde{p}) \tag{26}$$

Formally, this may be solved as follows:

$$\Lambda(\tilde{k},\,\tilde{p}) = \frac{V'(\tilde{k}-\tilde{p})}{\left\{1 \;-\; \frac{1}{\boldsymbol{\mathcal{V}}\beta}\sum_{\tilde{q},\,\lambda_{ph}}\Big[V'(\tilde{k}-\tilde{q})\Big]G_{\uparrow}^{0}(\tilde{q})G_{\downarrow}^{0}(-\tilde{q})\frac{\Lambda(\tilde{q},\,\tilde{p})}{\Lambda(\tilde{k},\,\tilde{p})}\right\}} \tag{27}$$

Equation (27) demonstrates the instability behavior when the 2nd denominator term approaches unity from the lower or upper sides. Refer to this equation as the Cooper vertex equation with its implicit stability behavior.

With the vertex explicitly stated in (27), one readily identifies the instability condition and obtains the Cooper instability equation, from equation (27) by setting the denominator to unity,

$$1 \;-\; \frac{1}{\boldsymbol{\mathcal{V}}\beta}\sum_{\tilde{q},\,\lambda_{ph}}\Big[V'(\tilde{k}-\tilde{q})\Big]G_{\uparrow}^{0}(\tilde{q})G_{\downarrow}^{0}(-\tilde{q})\frac{\Lambda(\tilde{q},\,\tilde{p})}{\Lambda(\tilde{k},\,\tilde{p})} = 0 \tag{28}$$

which should be evaluated at $T = T_c$, the critical temperature, since we expect the major physical change to occur here, and should be associated with the singularity. For the vertex function depending approximately only on its second variable, here $\tilde{p}$, the instability condition becomes

$$1 \;-\; \frac{1}{\boldsymbol{\mathcal{V}}\beta_c}\sum_{\tilde{q},\,\lambda_{ph}}\Big[V'(\tilde{k}-\tilde{q})\Big]G_{\uparrow}^{0}(\tilde{q})G_{\downarrow}^{0}(-\tilde{q}) = 0 \tag{29}$$

which may be rewritten as

$$1 \;=\; \frac{1}{\boldsymbol{\mathcal{V}}\beta_c}\sum_{\substack{iq_n \\ |iq_n|<\alpha\omega_D}}\;\sum_{\mathbf{q}}\;\sum_{\lambda_{ph}}\Big[V'(\tilde{k}-\tilde{q})\Big]G_{\uparrow}^{0}(\tilde{q})G_{\downarrow}^{0}(-\tilde{q}) \tag{30}$$

Here q_n is the Fermion index used in Matsubara reciprocal space imaginary frequency summations,

$$q_n = \frac{(2n+1)\pi}{\beta_c} = \frac{2\pi}{\beta_c}\left(n+\frac{1}{2}\right) \quad ; \quad \beta_c \;=\; \frac{1}{k_B T_c} \tag{31}$$

Bare Green's functions are

$$G_{\uparrow}^{0}(\mathbf{q},\,iq_n) = \frac{1}{iq_n \;-\; \xi_{\mathbf{q}\uparrow}} \quad ; \quad G_{\downarrow}^{0}(\mathbf{q},\,iq_n) = \frac{1}{iq_n \;-\; \xi_{\mathbf{q}\downarrow}} \tag{32}$$

Considering the case with no static or otherwise background magnetic field,

$$\xi_{\mathbf{q}\uparrow} \;=\; \xi_{\mathbf{q}\downarrow} \;=\; \xi_{\mathbf{q}} \tag{33}$$

Placing (32) and (33) into (30) then gives,

$$1 \;=\; \frac{1}{\boldsymbol{\mathcal{V}}\beta_c}\sum_{\substack{iq_n \\ |iq_n|<\alpha\omega_D}}\;\sum_{\mathbf{q}}\;\sum_{\lambda_{ph}}\Big[V'(\tilde{k}-\tilde{q})\Big]\frac{1}{iq_n \;-\; \xi_{\mathbf{q}}}\frac{1}{-\,iq_n \;-\; \xi_{\mathbf{q}}} \tag{34}$$

The disorder effect contributes an extra diagram ● = ⇒✱ = ⇒● for renormalized impurity scattering to the effective potential energy due to the Coulomb scattering offsetting the attractive electron-electron phonon mediated scattering:

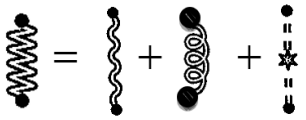

(35)

or

$$V_{eff}^{RPA,\,ren} = W^{Coul,\,RPA\,,\,ren}(\mathbf{q},\,iq_n) + \frac{1}{\boldsymbol{\nu}}\left|g_{\mathbf{q}\lambda}^{RPA,\,ren}\right|^2 D_{\lambda}^{RPA,\,ren}(\mathbf{q},\,iq_n) + W^{imp\ 1BA,\,RPA}(\mathbf{q},\,iq_n) \tag{36}$$

where the last term is given in the 1st Born approximation when only scattering off of a single impurity scatterer is allowed (Born approximation), and it is limited to one scattering event (1st). Under these assumptions, valid when scattering due to impurities is not too severe, the last term for impurity potential interaction energy is [Bruus and K. Flensberg, 2004]

$$W^{imp\ 1BA,\,RPA}(\mathbf{q},\,iq_n) = n_{imp}\frac{u(\mathbf{q})}{\varepsilon^{RPA}(\mathbf{q},\,0)}\frac{u(-\mathbf{q})}{\varepsilon^{RPA}(-\mathbf{q},\,0)}\delta_{q_n,\,0} \tag{37}$$

which we see has the renormalized impurity interaction lines for incoming q and outgoing – q momentum into the impurity center vertex, weighted by the impurity spatial density n_{imp}, which arises from the summation over all scatterers per unit volume. The Kronecker delta function, forces one to consider Matsubara frequencies approaching zero.

In a hierarchy of approximations, with various physical effect ramifications, one simplification is to pull $V'(\tilde{k}-\tilde{q})$ out from under the **q** and λ_{ph} summation signs, replacing it by an average. This process is consistent with the earlier two variable to one variable vertex function simplification, which suggests here we drop dependence on **k**.

$$1 = \frac{V'_{av}}{\boldsymbol{\nu}\beta_c}\sum_{\substack{iq_n \\ |iqn|<\alpha\omega_D}}\sum_{\mathbf{q}}\frac{1}{iq_n - \xi_{\mathbf{q}}}\frac{1}{-iq_n - \xi_{\mathbf{q}}} \tag{38}$$

Here the λ_{ph} summation has been dropped entirely (and absorbed into V'_{av}) since the remaining bare Green's function contains no phonon polarization information. The **q** summation is implicitly over one spin type, where $\xi_{\mathbf{q}}$ is taken above ($\xi_{\mathbf{q}} > 0$)and below ($\xi_{\mathbf{q}} < 0$) the Fermi surface. Above the Fermi surface $\xi_{\mathbf{q}}$ is unbounded, but below it can go to, at least in a normal 3D metal, to $-\epsilon_F$. Therefore, using the density of states $d_{st}(\xi)$, (38) becomes

$$\begin{aligned}
1 &= \frac{V'_{av}}{\boldsymbol{\nu}\beta_c}\sum_{\substack{iq_n \\ |iq_n|<\alpha\omega_D}}\sum_{\mathbf{q}}\frac{1}{iq_n - \xi_{\mathbf{q}}}\frac{1}{-iq_n - \xi_{\mathbf{q}}} \\
&= \frac{V'_{av}}{\boldsymbol{\nu}\beta_c}\sum_{\substack{iq_n \\ |iq_n|<\alpha\omega_D}}\frac{1}{\boldsymbol{\nu}}\sum_{\mathbf{q}}\frac{1}{iq_n - \xi_{\mathbf{q}}}\frac{1}{-iq_n - \xi_{\mathbf{q}}} \\
&= \frac{V'_{av}}{\beta_c}\sum_{\substack{iq_n \\ |iq_n|<\alpha\omega_D}}\frac{1}{2}\int_{-\varepsilon_F}^{\infty} d_{st}(\xi)d\xi\frac{1}{iq_n - \xi_{\mathbf{q}}}\frac{1}{-iq_n - \xi_{\mathbf{q}}} \\
&= \frac{V'_{av}}{\beta_c}\sum_{\substack{iq_n \\ |iq_n|<\alpha\omega_D}}\frac{1}{2}\int_{-\varepsilon_F}^{\infty} d_{st}(\xi)d\xi\frac{1}{(q_n)^2 + \xi^2} \\
&\approx \frac{V'_{av}}{\beta_c}\sum_{\substack{iq_n \\ |iq_n|<\alpha\omega_D}} d_{st}(\xi=0;\,\varepsilon=\varepsilon_F)\frac{1}{2}\int_{-\varepsilon_F}^{\infty} d\xi\frac{1}{(q_n)^2 + \xi^2} \\
&\approx \frac{V'_{av}}{\beta_c}\sum_{\substack{iq_n \\ |iq_n|<\alpha\omega_D}} d_{st}(\xi=0;\,\varepsilon=\varepsilon_F)\frac{1}{2}\int_{-\infty}^{\infty} d\xi\frac{1}{(q_n)^2 + \xi^2} \\
&= \frac{V'_{av}}{\beta_c}\sum_{\substack{iq_n \\ |iq_n|<\alpha\omega_D}}\frac{d_{st}(\varepsilon_F)}{2}\frac{1}{q_n}\tan^{-1}\left(\frac{\xi}{q_n}\right)\Bigg|_{-\infty}^{+\infty} \\
&= \frac{V'_{av}}{\beta_c}\sum_{\substack{iq_n \\ |iq_n|<\alpha\omega_D}}\frac{d_{st}(\varepsilon_F)}{2}\frac{2}{q_n}\tan^{-1}(\infty)\mathrm{sgn}(q_n) \\
&= \frac{V'_{av}}{\beta_c}\sum_{\substack{iq_n \\ |iq_n|<\alpha\omega_D}}\frac{d_{st}(\varepsilon_F)}{2}\frac{2}{|q_n|}\frac{\pi}{2}
\end{aligned} \tag{39}$$

The final result obtained from the last line of equation (39), is a double-sided sum over Matsubara frequencies. The idea is to convert this into a single sided sum, convert that into an integral, and recognize a familiar form which has an analytical reduction. From (39) we write

$$1 = \frac{V'_{av}}{2\beta_c}\sum_{\substack{iq_n \\ |iq_n|<\alpha\omega_D}} d_{st}(\varepsilon_F)\frac{\pi}{|q_n|} = \frac{V'_{av}d_{st}(\varepsilon_F)}{2\beta_c}\sum_{\substack{iq_n \\ |iq_n|<\alpha\omega_D}}\frac{\pi}{|q_n|} \tag{40}$$

[Note that the earlier DOS $d(e_F)$, and $d_{st}(e_F)$, are identical, with the additional subscript merely serving to emphasize the distinction from the differential operator inside the integral.] Carrying out the steps outlined, using the Fermion frequency index relation (31),

$$\begin{aligned}
1 &= \frac{V'_{av} d_{st}(\varepsilon_F)}{2\beta_c} \sum_{\substack{iq_n \\ |iq_n|<\alpha\omega_D}} \frac{\pi}{|q_n|} \\
&= \frac{V'_{av} d_{st}(\varepsilon_F)}{2\beta_c} \sum_{\substack{iq_n \\ |iq_n|<\alpha\omega_D}} \frac{\pi}{\left|\frac{(2n+1)\pi}{\beta_c}\right|} \\
&= \frac{V'_{av} d_{st}(\varepsilon_F)}{2\beta_c} \sum_{\substack{iq_n \\ |iq_n|<\alpha\omega_D}} \frac{\beta_c}{2} \frac{1}{|n+1/2|} \\
&= \frac{V'_{av} d_{st}(\varepsilon_F)}{2\beta_c} \frac{\beta_c}{2} \sum_{\substack{iq_n \\ |iq_n|<\alpha\omega_D}} \frac{1}{|n+1/2|} \\
&= \frac{V'_{av} d_{st}(\varepsilon_F)}{4} \sum_{\substack{n=0,\pm1,\pm2,.. \\ |iq_n|<\alpha\omega_D}} \frac{1}{|n+1/2|} \\
&= \frac{V'_{av} d_{st}(\varepsilon_F)}{4} \left\{ \sum_{\substack{n=0,1,2,.. \\ |iq_n|<\alpha\omega_D}} \frac{1}{n+1/2} + \sum_{\substack{n=-1,-2,.. \\ |iq_n|<\alpha\omega_D}} \frac{1}{|n+1/2|} \right\} \\
&= \frac{V'_{av} d_{st}(\varepsilon_F)}{4} \left\{ \sum_{n=0}^{\alpha\beta_c\omega_D/(2\pi)-1/2} \frac{1}{n+1/2} + \sum_{n=-1}^{-\alpha\beta_c\omega_D/(2\pi)-1/2} \frac{1}{|n+1/2|} \right\} \\
&= \frac{V'_{av} d_{st}(\varepsilon_F)}{4} 2 \sum_{n=0}^{\alpha\beta_c\omega_D/(2\pi)-1/2} \frac{1}{n+1/2}
\end{aligned} \tag{41}$$

So we have obtained a single-sided sum as desired,

$$1 = \frac{V'_{av} d_{st}(\varepsilon_F)}{2} \sum_{n=0}^{\alpha\beta_c\omega_D/(2\pi)-1/2} \frac{1}{n+1/2} \tag{42}$$

One way to handle this summation is to replace it by an integral approximation, taking $1 \to dn$, and perform a change of variable, so that

$$\begin{aligned}
1 &\approx \frac{V'_{av} d_{st}(\varepsilon_F)}{2} \int_0^{\alpha\beta_c\omega_D/(2\pi)-1/2} \frac{dn}{n+1/2} \\
&= \frac{V'_{av} d_{st}(\varepsilon_F)}{2} \int_{1/2}^{\alpha\beta_c\omega_D/(2\pi)-1/2+1/2} \frac{dm}{m} \\
&= \frac{V'_{av} d_{st}(\varepsilon_F)}{2} \ln(m)\Big|_{1/2}^{\alpha\beta_c\omega_D/(2\pi)} \\
&= \frac{V'_{av} d_{st}(\varepsilon_F)}{2} \left[\ln\left(\frac{\alpha\beta_c\omega_D}{2\pi}\right) - \ln\left(\frac{1}{2}\right) \right] \\
&= \frac{V'_{av} d_{st}(\varepsilon_F)}{2} \ln\left(\frac{\alpha\beta_c\omega_D}{\pi}\right)
\end{aligned} \tag{43}$$

or

$$1 = \frac{V'_{av} d_{st}(\varepsilon_F)}{2} \ln\left(\frac{\alpha\beta_c\omega_D}{\pi}\right) \tag{44}$$

Equation (44) may be solved using (36) broken into two pieces, instead of three, the electron-electron and the electron-phonon renormalization terms collected together, and the impurity disorder contribution:

$$V'^{RPA,\,CP}_{eff}(\mathbf{q}, iq_n) = W^{Coul,\,RPA\,,\,ren}(\mathbf{q}, iq_n) + \frac{1}{\nu} \left| g^{RPA,\,ren}_{\mathbf{q}\lambda} \right|^2 D^{RPA,\,ren}_{\lambda}(\mathbf{q}, iq_n) \tag{45}$$

$$V'^{RPA,\,imp}_{eff} = W^{imp\ 1BA,\,RPA}(\mathbf{q}, iq_n) \tag{46}$$

to make the total as

$$V'^{RPA,\,ren}_{eff} = V'^{RPA,\,CP}_{eff} + V'^{RPA}_{imp} \tag{47}$$

Notice that $V'^{RPA,\,CP}_{eff}$ of (45) is just the $V'^{RPA,\,CP}_{eff}$ identified elsewhere as

$$V^{RPA,\,ren}_{eff} = W^{Coul,\,RPA\,,\,ren}(\mathbf{q},\, iq_n) + \frac{1}{\boldsymbol{\mathcal{V}}}\left|g^{RPA,\,ren}_{\mathbf{q}\lambda}\right|^2 D^{RPA,\,ren}_{\lambda}(\mathbf{q},\, iq_n) \tag{48}$$

which shows the right-hand-sides of both equations are identical. When this decomposition is done, the solution to (44) may be written as

$$T_c = T_c^{\alpha}\Big|_{\substack{BCS\\pre}}\left(T_c\Big|_{\substack{BCS\\\exp}}\right)^{\gamma_{rp}} \tag{49}$$

where the following definitions are used:

$$T_c^{\alpha}\Big|_{\substack{BCS\\pre}} = \frac{\alpha}{\pi}\frac{\hbar\omega_D}{k_B}\;;\; T_c\Big|_{\substack{BCS\\\exp}} = e^{-\frac{2}{V'^{RPA,\,CP}_{eff,\,av}}\frac{1}{d(\varepsilon_F)}}\;;\; \gamma_{rp} = \frac{1}{1 + V'^{RPA}_{imp,\,av}/V'^{RPA,\,CP}_{eff,\,av}} \tag{50}$$

The next thing is realize that other mechanisms besides impurity scattering, phonon energy exchange, Coulomb scattering and repulsion, may be acting. This could include charge density waves to move energy into the Cooper pairs, spin density waves to again move energy into the Cooper pairs, plasma oscillations to impart energy to the Copper paired electrons, as well as other energy imparting mechanisms. Therefore, (45) should be ungraded to read

$$V'^{RPA,Tot}_{eff}(\mathbf{q}, iq_n) = W^{Coul,RPA,ren}(\mathbf{q}, iq_n) + \sum_m \frac{1}{\boldsymbol{V_{vol}}}\left|g^{RPA,ren}_{\mathbf{q},m}\right| D^{RPA,ren}_{m}(\mathbf{q}, iq_n) \tag{51}$$

Here the total energy of interaction $V'^{RPA,Tot}_{eff}(\mathbf{q}, iq_n)$ includes a summation over all energy exchange mechanismsm. Once (51) is realized, (49) and (50) are no longer correct, but also must be enhanced to include all the active energy exchange mechanisms.

$$T_C = T_C^{\alpha}\Big|_{\substack{m\\pre}}\left(T_C\Big|_{\substack{m\\exp}}\right)^{\gamma_{rp,m}} \tag{52}$$

where the following new definitions are used:

$$T_C^{\alpha}\Big|_{\substack{m\\pre}} = \frac{\alpha}{\pi}\frac{\hbar\omega_D}{k_B}\;;\; T_C\Big|_{\substack{m\\exp}} = e^{-\frac{2}{V'^{RPA,Tot}_{eff,av}}\frac{1}{d(\varepsilon_F)}}\;;\; \gamma_{rp,m} = \frac{1}{1 + V'^{RPA}_{imp,av}/V'^{RPA,Tot}_{eff}} \tag{53}$$

To be strictly correct, $\hbar\omega_D$ depends on each energy exchange mechanismm , and so it really reads as $\hbar\omega_{D_m}$, and thus re-embeds into the earlier equations, considerably complicating the analysis (which has been done elsewhere), without damaging the overall insights. What is learned from (52) and (53) is that accumulating more energy exchange mechanisms, reduces the damage from the second factor in (52), thereby allowing the first factor to become more dominant. Furthermore, if one eliminates the impurity scattering effect of the third exponential power in (53), setting it to unity

$$\gamma_{rp,m} \rightarrow 1 \tag{54}$$

the simplified form for the critical temperature arises.

$$T_C = T_C^{\alpha}\Big|_{\substack{m\\pre}} T_C\Big|_{\substack{m\\exp}} \tag{55}$$

Now, without the issue of impurity scattering, one sees that T_C may be more readily elevated by constructing new unit cell superconducting crystal structures which enhance various energy exchange mechanisms, for transferring energy from each identified mechanism into the Cooper paired electrons.

Conclusions

In this treatment, a very different approach has been taken, to become informed about ways to overcome the impasse for reaching very high critical temperatures for superconductivity. First, one delved into carrier transport and the attendant band structures, to gain insights. This took us into the realm of semiconductor integrated circuits for electronics, a vast and rich area of research, engineering and manufacturing of transistors and their uses in a multiplicity of devices. With this background, attention was directed at RF electronics, and in particular power RF electronics. This gave us an impetus for altering the backbone atoms of high temperature superconductors, like the cuprate superconductors. Studied were replacing nonmetal atoms of oxygen with other nonmetal atoms, with insights gained from previous examination here of the RF power electronics.

Then focus was directed toward the charge sharing atoms, which provide carriers for the conducting planes or track atoms. Finally, an extensive examination of possible conducting track atoms for replacing, say copper atoms in cuprate SCs, with other atoms, was undertaken. Many possible atoms were found, considering covalent radaii, valencies, and availability of the atoms in the crust. Having gone through this study exercise, it has become apparent that there may be still many possibilities to break through the seemingly impossible barrier of near room temperature T_c performance. This barrier to getting to 300 K operation, is the value of a T_c under standard pressure, of 200 K. Once that realistic barrier can be penetrated, the insights gained will guide the way forward to near room temperature superconductivity operation. In order to gain some appreciation of the impetus for the study conducted herein, the implicit additive nature of the energy exchange mechanisms to the increase of T_c was delineated by examining the Cooper instability equation. By performing the various solid state chemistry initiatives suggested in the study presented here, increases in or new additions to the energy exchange mechanisms, may become possible.

References

1. Vurgaftman, I., Meyer, J.R., Ram-Mohan, L.R. (2001). Band parameters for III–V compound semiconductors and their alloys. Journal of Applied Physics, 89(11), 5815-5875.
2. Sze, S.M. (1969). Physics of Semiconductor Devices. Wiley.
3. Large, N. (2011). Resonant Raman-Brillouin scattering in semiconductor and metallic nanostructures: From nano-acoustics to acousto-plasmonics. Ph.D. Thesis, Université de Toulouse and Universidad del País Vasco.
4. Krowne, C.M., Holm-Kennedy, J.W. (1972). Electron energy losses at an inverted p-type (100) silicon surface at liquid helium temperatures assuming two- and three-dimensional motion. Bulletin of the American Physical Society, 17, 1195.
5. Holm-Kennedy, J.W., Matthews, D., Krowne, C.M. (1973). The effect of mobility anisotropy on transverse voltage generation in IGFETs. Bulletin of the American Physical Society, 19, 1605.
6. Krowne, C.M., Holm-Kennedy, J.W. (1974). Energy relaxation of electrons in the (100) n-channel of a Si-MOSFET. I. Bulk phonon treatment. Surface Science, 46, 197-231.
7. Krowne, C.M., Holm-Kennedy, J.W. (1974). Energy relaxation of electrons in the (100) n-channel of a Si-MOSFET. II. Surface phonon treatment. Surface Science, 46, 232-250.
8. Krowne, C.M. (1975). Electron energy relaxation at the Si-SiO_2 interface of a (100) n-channel Si-MOSFET device. Ph.D. Dissertation, Department of Electrical Sciences and Engineering, University of California, Los Angeles, https://www.proquest.com/openview/f51d810466020fc5fff4800910b64766/1?pq-origsite=gscholar&cbl=18750&diss=y.
9. Krowne, C.M. (1983). Electron power loss in the (100) n-channel of a Si metal oxide semiconductor field effect transistor. I. Intrasubband phonon scattering. Journal of Applied Physics, 54, 2441-2454.
10. Krowne, C.M. (1983). Electron power loss in the (100) n-channel of a Si metal oxide semiconductor field effect transistor. II. Intersubband phonon scattering. Journal of Applied Physics, 54, 2455-2467.
11. Krowne, C.M., Cukauskas, E.J. (1987). GaAs slow wave phase shifter characteristics at cryogenic temperatures. IEEE Transactions on Electron Devices, ED-34, 124-129.
12. Krowne, C.M., Blakey, P.A. (1987). On the existence of submillimeter-wave negative conductance in n-gallium arsenide diodes. Journal of Applied Physics, 61, 2257-2266.
13. Krowne, C.M. (1987). Analytical method for selecting random scattering angle for polar or acoustic phonon scattering of central valley conduction band electrons in GaAs. IEE Proceedings I: Solid-State Electron Devices, 134, 45-50.
14. Krowne, C.M., Thompson, P.E. (1987). Ion-implanted GaAs slow wave monolithic structure. Solid-State Electronics, 30, 497-502.
15. Krowne, C.M., Cukauskas, E.J. (1987). Cryogenic operation of a monolithic slow wave variable phase shifter. IEEE Transactions on Microwave Theory and Techniques, MTT-35, 868-871.
16. Tait, G.B., Krowne, C.M. (1987). Efficient TED simulation method for microwave and millimeter wave CAD applications. Solid-State Electronics, 30, 1025-1036.
17. Tait, G.B., Krowne, C.M. (1987). Determination of transport parameters for InP device simulations in n^+nn^+ structures. Solid-State Electronics, 30, 1317-1322.
18. Krowne, C.M. (1988). Analytical representation of impedance using the Boltzmann equation for nonlinear two-terminal device behavior. Physical Review B, 37, 891-897.
19. Krowne, C.M. (1988). Nonlinear large signal admittance in n-GaAs diodes at terahertz frequencies based upon transport analysis. Journal of Applied Physics, 64, 2160-2163.
20. Krowne, C.M., Tait, G.B. (1989). Propagation in layered biased semiconductor structures based on transport. IEEE Transactions on Microwave Theory and Techniques, MTT-37, 711-722.
21. Krowne, C.M. (1989). Semiconductor heterostructure nonlinear Poisson equation. Journal of Applied Physics, 65, 1602-1614.
22. Krowne, C.M., Blakey, P.A. (1993). Submillimeter wave low temperature admittance of n-GaAs and n-InP diode structures. Journal of Applied Physics, 74(4), 2633-2637.
23. Krowne, C.M., Ikossi-Anastasiou, K., Kougianos, E. (1995). Early voltage in heterojunction bipolar transistors: Quantum tunneling and base recombination effects. Solid-State Electronics, 38(12), 1979-1991.
24. Buot, F.A., Krowne, C.M. (1999). A double barrier THz source based on electrical excitation of electrons and holes. Journal of Applied Physics, 86(9), 5215-5231.
25. Buot, F.A., Zhao, P., Cui, H.L., Woolard, D.L., Jensen, K.L., et al. (2000). Emitter quantization and double hysteresis in resonant-tunneling structures: A nonlinear model of charge oscillation and current bistability. Physical Review B, 61(8), 5644-5665.

26. Suzuki, M., Uenoyama, T., Yanase, A. (1995). First-principles calculations of effective-mass parameters of AlN and GaN. Physical Review B, 52(11), 8132-8139.
27. Bloom, S., Harbeke, G., Meier, E., Ortenburger, I.B. (1974). Band structure and reflectivity of GaN. Physica Status Solidi, 66, 161-168.
28. Pennington, G., Goldsman, N. (2004). Self-consistent calculations for n-type hexagonal SiC inversion layers. Journal of Applied Physics, 95(8), 4223-4234.
29. Morkoç, H. (1994). Large-band-gap SiC, III-V nitride, and II-VI ZnSe-based semiconductor device technologies. Journal of Applied Physics, 76(3), 1363-1398.
30. Kelly, J.F., Fisher, G.R., Barnes, P. (2005). Correlation between layer thickness and periodicity of long polytypes in silicon carbide. Materials research bulletin, 40(2), 249-255.
31. Laine, R.M. (1993). Preceramic polymer routes to silicon carbide. Chemistry of Materials, 5(3), 260-279.
32. Ramsdell, L.S. (1945). Studies on silicon carbide. American Mineralogist, 32, 64-82.
33. Loret, B., Forget, A., Moussy, J.B., Poissonnet, S., Bonnaillie, P., et al. (2017). Crystal growth and characterization of $HgBa_2Ca_2Cu_3O_{8+\delta}$ superconductor with the highest critical temperature at ambient pressure. Inorganic Chemistry, 56, 9396-9399.
34. Chmaissem, O., Huang, Q., Antipov, E.V., Putilin, S.N., Marezio, M., et al. (1993). Neutron powder diffraction study at room temperature and at 10 K of the crystal structure of the 133 K superconductor $HgBa_2Ca_2Cu_3O_{8+\delta}$. Physica C: Superconductivity, 217(3-4), 265-272.
35. Antipov, E.V., Capponi, J.J., Chaillout, C., Chmaissem, O., Loureiro, S.M., et al. (1993). Synthesis and neutron powder diffraction study of the superconductor $HgBa_2CaCu_2O_{6+\delta}$ before and after heat treatment. Physica C: Superconductivity, 218, 348-355.
36. Shao, H.M., Lam, C.C., Fung, P.C.W., Wu, X.S., Du, J.H., et al. (1995). The synthesis and characterization of $HgBa_2Ca_2Cu_3O_{8+\delta}$ superconductors with substitution of Hg by Pb. Physica C: Superconductivity, 246(3-4), 207-215.
37. Dai, P., Chakoumakos, B.C., Sun, G.F., Wong, K.W., Xin, Y., et al. (1995). Synthesis and neutron powder diffraction study of the superconductor $HgBa_2Ca_2Cu_3O_{8\delta}$ by Tl substitution. Physica C: Superconductivity, 243(3-4), 201-206.
38. Rotter, M., Tegel, M., Johrendt, D. (2008). Superconductivity at 38 K in the iron arsenide $(Ba_{1-x}K_x)Fe_2As_2$. Physical Review Letters, 101(10), 107006.
39. Tarantini, C., Limon, S.A., Mao, K., Hellstrom, E.E., Kametani, F. (2025). Evidence of multiscale supercurrents in K-doped $BaFe_2As_2$. Superconductor Science and Technology, 38, 045023.
40. Sasmal, K., Lv, B., Lorenz, B., Guloy, A.M., Chen, F., et al. (2008). Superconducting Fe-based compounds $(A_{1-x}Sr_x)Fe_2As_2$ with A = K and Cs with transition temperatures up to 37 K. Physical Review Letters, 101(10), 107007.
41. Marra, P., Nigro, A., Li, Z., Chen, G.F., Wang, N.L., et al. (2012). Paraconductivity of the K-doped $SrFe_2As_2$ superconductor. New Journal of Physics, 14, 043001.
42. Krowne, C.M. (2017). Disorder Modifications of the Critical Temperature for Superconductivity: A Perspective from the Point of View of Nanoscience. In Advances in Imaging and Electron Physics 202(39-74), https://www.sciencedirect.com/science/article/pii/S1076567017300575.
43. Krowne, C.M. (2017). Critical Magnetic Field and Its Slope, Specific Heat, and Gap for Superconductivity as Modified by Nanoscopic Disorder. In Advances in Imaging and Electron Physics, 203(67-97), https://www.sciencedirect.com/science/article/pii/S1076567017300423.

Copyright: ©2026 Clifford M Krowne. This is an open-access article distributed under the terms of the Creative Commons Attribution License, which permits unrestricted use, distribution, and reproduction in any medium, provided the original author and source are credited.